Soft Matter

ARTICLE TYPE

Cite this: DOI: 10.1039/xxxxxxxxxx

A Reversible Viscoelastic Adhesive

Hugo Perrin*[a], Antonin Eddi[b‡], Stefan Karpitschka[c], Jacco H. Snoeijer[d] and Bruno Andreotti[a‡]

Received Date
Accepted Date

DOI: 10.1039/xxxxxxxxxx

www.rsc.org/journalname

The functionality of adhesives relies on their response under the application of a load. Yet, it has remained a challenge to quantitatively relate the macroscopic dynamics of peeling to the dissipative processes inside the adhesive layer. Here we consider a reversible adhesive consisting of a crosslinked polymer network, which is analysed by simultaneous measurement of small-scale deformation together with the peeling force and velocity. Experiments are complemented by a viscoelastic model based on the adhesive's rheology. We demonstrate the emergence of a "wetting" angle at the contact line and show how it gives access to a quantitative prediction of the scaling laws for peeling, in good agreement with experiment. Our findings provide a new strategy for design of reversible adhesives, by quantitatively combining wetting, geometry and dissipation.

1 Introduction

Pressure sensitive adhesives, ubiquitous for domestic and industrial applications, have the characteristic property that they do not undergo chemical reactions during the bonding process and their performance life. Animals with adhesive pads are ubiquitous in nature[1] and have inspired numerous designs of artificial reversibly adhesive materials[2–5]. The insights combining viscoelasticity, capillarity, and multiscale hierarchical topography[6] are crucial to design innovative adhesives. Namely, an effective adhesive material should stick under physical contact with a substrate and must therefore respond highly compliant, similar to a liquid. Its adhesive performance results from the resistance to peeling it off a substrate. Strong adhesion implies a high energy dissipation, produced in most polymeric materials by fingering instabilities[7–10], cavitation[11] and fibrillar deformation.

From a theoretical perspective, pioneering models have considered the opposite limit of weak adhesion, for which the debonding is interfacial, reversible, and the adhesives remain weakly deformed[12]. According to these theories[13–21], the dissipation during debonding can be related to the linear viscoelastic properties of the adhesive[17,22]. The recent review by Creton and Ciccotti[2] gives a comprehensive overview of the development of the field. Most experiments with peeling adhesive tapes[23,24] or bulk fracture[25] disagree quantitatively with theoretical predictions[21,26,27]. This leaves a gap in first principles understanding, and has led to the conclusion that non-linear viscoelastic dissipation and, most often, damage mechanisms in the polymer network should be taken into account[2,28].

In this paper we investigate the dynamics of peeling for a reversible viscoelastic adhesive, which can be peeled off without exhibiting irreversible plastic damage (Fig. 1). Rather than considering the classical case of peeling a thin, strong adhesive with a flexible backing off a rigid solid[7,23,24,29], we take the opposite perspective: we use a thick layer of a weak adhesive on a rigid backing and peel off a thin flexible tape of a much stiffer material (cf. Fig. 1). This way, we disentangle the effects of bending elasticity, viscoelastic dissipation, and adhesion energy. Our model adhesive is made of a multi-scale polymer gel, whose strong dissipation is controlled by linear viscoelasticity. The key finding is that the dissipation in the bulk is determined by the singular deformation in the vicinity of the contact line, this singularity being regularised by surface energy. This is in stark contrast to "classical" peeling where the blunt and frequently irregular crack front cannot localize dissipation sufficiently and the thickness of the adhesive matters[2]. We propose a quantitative theory that resolves all our experimental findings in detail, based on which we establish new scaling laws for peeling of such reversible adhesives.

2 Set-up

Elastomers are reticulated polymers obtained by cross-linking long polymer chains. The longer the chains between cross-links (or entanglement points), the larger their relaxation timescale and their effective viscosity. Here we use an addition-cure adhesive that consists of a Silicone gel (Dow Corning CY52-276) whose reticulated polymer network is formed by polymerizing

[a] Laboratoire de Physique Statistique (LPS), UMR 8550 CNRS, ENS, Univ. Paris Diderot, Sorbonne Université, 24 rue Lhomond, 75005, Paris, France.
[b] Laboratoire de Physique et Mécanique des Milieux Hétérogènes (PMMH), UMR 7636 CNRS, ESPCI, Univ. Paris Diderot, Sorbonne Université, 10 rue Vauquelin, 75005 Paris, France
[c] Max Planck Institute for Dynamics and Self-Organization, Am Fassberg 17, 37077 Goettingen, Germany
[d] Physics of Fluids Group, Faculty of Science and Technology, University of Twente, P.O. Box 217, 7500 AE Enschede, The Netherlands

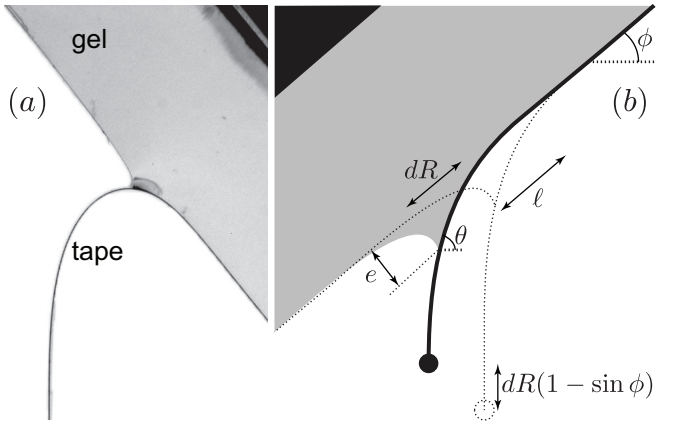

Fig. 1 (a) Image of the peeling experiment. A tape is pulled vertically from the adhesive gel under the influence of a weight (not in the image) pending at its end. (b) Schematic illustrating the gravitational energy released by a peeling a length dR. The forcing is controlled by varying the attached mass and the inclination ϕ. The image also defines the normal deflection e, the lateral scale $\ell = (B/G)^{1/3}$ on the side where the tape is still attached, and the tape inclination at the contact line θ.

small multifunctional prepolymers. At the gel point, a fractal polymer network forms, which is composed of branches of all lengths between the prepolymer and the size of the sample. We mix the two components at the stoichiometric ratio of 1:1 (A:B), providing extra cross-links with respect to the gel point and leading to a finite shear elastic modulus $G \simeq 1.2$ kPa. The linear rheology is very accurately fitted by the simple relation

$$\mu(\omega) = G'(\omega) + iG''(\omega) = G\left[1 + (i\tau\omega)^n\right], \qquad (1)$$

with an exponent $n \simeq 0.55$. This bulk rheology obey Kramers-Kronig relation: both the storage and the loss moduli originate from the same relaxation function $G\left[1+\Gamma(1-n)^{-1}(\tau/t)^n\right]$, where Γ is the gamma function. The power law dependence of the loss modulus $G'' \sim \omega^n$ reflects the architecture of the polymer network, with a continuum distribution of relaxation times[30]. The cross-over timescale, measured $\tau = 0.13$ s for our system, is determined by the length of largest branches of polymers in the network. Once stirred and degassed, the mixture of the two prepolymers is poured into petri dishes to make gel layers of varying thickness (from $2-10$ mm).

A thin, virtually inextensible film of bending modulus B is placed on the gel, and is subsequently peeled off at controlled forcing. The experiment is performed by placing the system upside-down, inclined at a variable angle ϕ with respect to the horizontal[31], and attaching a mass at the end of the tape (Fig. 1). The forcing is varied by four orders of magnitude by using different masses and also by peeling due to the weight of the plastic sheet alone. The sheet's bending modulus B was varied by one order of magnitude by using two types of tape: a $88\,\mu$m thick biaxially oriented polypropylene film (BOPP manufactured by Innovia) and a $34\,\mu$m thick Mylar film (Polyethylene terephthalate) coated with Aluminium (PET, manufactured by Toray). The tapes are smooth at optical scales – submicrometer roughness could not be measured. Despite no further annealing was applied, the samples did not present any plastic damage nor any spontaneous curvature. The position of the contact line, where the sheet joins the gel, and the geometry of the ridge formed below this contact line are recorded using a video camera (1024×1024 pixels with a resolution of $20\,\mu$m/pix).

The key control parameter of the experiment is the peeling force f per unit width, defined as the energy released by gravity when the contact line moves by a unit distance. To quantify this force, we focus on the case where the length R of the freely pending tape is sufficiently large to be quasi vertical close to its free end. Then, peeling the tape by a length dR, the end of the tape moves downward by $dR(1-\sin\phi)$ [c.f. Fig. 1(b)]. Hence, we obtain the peeling force per unit width:

$$f = \lambda g(1-\sin\phi), \qquad (2)$$

where λ is the mass at the end of the tape per unit width. In this expression we neglected the weight of the sheet, which can also be included as required (see Appendix B).

3 Geometric characteristics of the peeling front

The present setup provides an experimental access to the geometric features in the vicinity of the contact line[32]. This is of key importance to understand the viscoelastic dissipation during the peeling, which occurs as the highly deformed zone travels along the gel. For the studied parameters, the peeling front remains straight and stable: no oscillation nor stick-slip motion like those reported by Cortet & al.[33] were observed. The peeling dynamics reaches a steady travelling state after a transient that lasts less than a second for the largest velocities. The geometric aspects can be inferred from Fig. 1 (b). Interestingly, the typical scales of deformation, e in the normal direction and ℓ parallel to the gel layer, depend non-trivially on f. In Fig. 2 we plot the normal displacement e as a function of forcing f, at different inclination angles ϕ. The response is far from linear, with a scaling law $e \sim f^{1/2}$, even though typical strains are within the linear range of the gel.

This nonlinear response of the normal displacement can be understood in two steps. First, we analyze the part of the elastic gel that is in contact with the tape. The gel layer is soft and thick, and characterized by its (static) shear modulus G. A surface deflection of amplitude e and horizontal scale ℓ induces a normal stress $\sigma \sim Ge/\ell$. By contrast, the elasticity of the thin, stiff tape is characterized by its bending modulus B, and gives a typical normal stress $\sigma \sim Be/\ell^4$. The balance of stress thus does not select the normal deflection e, but provides access to a lateral length scale ℓ given by:

$$\ell = \left(\frac{B}{G}\right)^{1/3}. \qquad (3)$$

This elasto-bending length ℓ is the wavelength of wrinkles that appear when compressing a soft foundation that is covered by a hard, thin skin[34,35]. In the present case of a peeling experiment, where the elastic film is under tension, ℓ represents the decay length over which the angle of the tape aligns to the gel layer (Fig. 1b).

We verify this explicitly by measuring, for each set of exper-

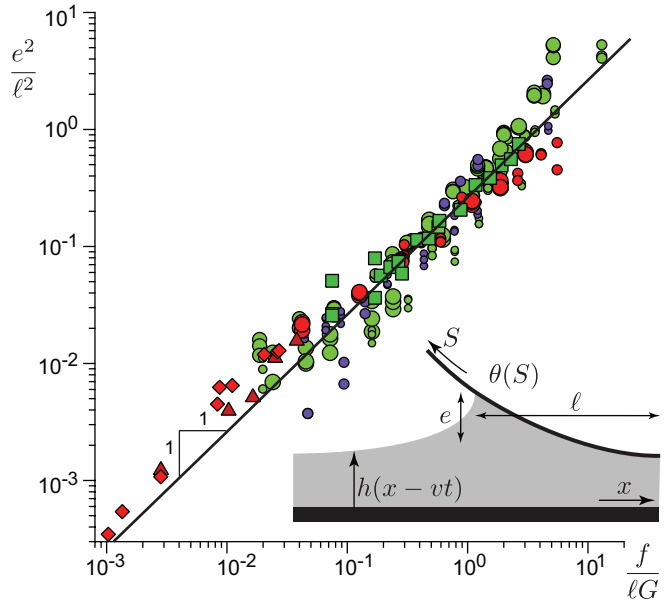

Fig. 2 Relation between the gel deformation e, rescaled by the elasto-bending length $\ell = (B/G)^{1/3}$, and the peeling force f rescaled by ℓ and by the gel elastic modulus G. The colors correspond to different inclination angles ϕ from red to blue ($-45°$, $0°$, $45°$) and the symbols to the type of experiment, as shown in Fig. 5. The marker's size codes for gel thickness. The data collapses according to (6) shown as the solid line (prefactor $\simeq 0.26$). Inset: the shape of the sheet is parametrised by θ, the shape of the gel by h.

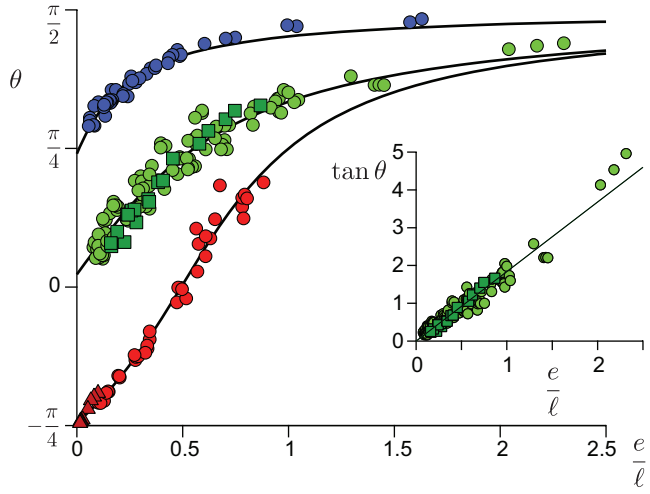

Fig. 3 Angle θ at the contact line as a function of the deformation e, rescaled by the elastic length ℓ. The data correspond to different types of tape and configurations. The colors correspond to the global inclination angle ϕ. The solid lines show the best fit by the form $\tan\theta = \tan\phi + e/(\alpha\ell)$. For red points $\phi = -45°$ and $\alpha = 0.51$, for green points $\phi = 0°$ and $\alpha = 0.6$, for blue points $\phi = 45°$ and $\alpha = 0.18$. Inset: slope $\tan\theta$ of the sheet at the contact line for $\phi = 0°$. The solid line indicates $\tan\theta \sim e/\ell$.

iments – type of tape, configuration (with or without a mass) and global inclination ϕ – the inclination of the tape at the contact line θ with respect to the horizontal, for different peeling forces (see Fig. 1b for the definition of θ). A very simple view of the deformation would be to approximate the tape as a triangle, with normal extension e and lateral extension on the side of the gel given by ℓ. This would give a geometric relation $\tan\theta - \tan\phi = (e/\ell)(1+\tan\theta\tan\phi)$. However, this approximation has the drawback that it does not capture the large deformation asymptotic: when $e \to +\infty$ we find that $\theta \to \pi/2$ since the tape is aligned with gravity already at the location of the contact line. Therefore we propose the fit:

$$\tan\theta - \tan\phi = \frac{e}{\alpha\ell}, \tag{4}$$

as it correctly gives the divergence of the normal deformation e when $\theta \to \pi/2$ and is consistent with the triangular model for $\phi = 0$. Figure 3 presents the angle θ as a function of the deformation e/ℓ for the different sets of experiments – the inset shows the case $\phi = 0$. The data are very well described by the fit (4) for all ϕ, shown as a solid lines. The prefactor α was found of order unity for all cases (see caption), and shows that ℓ as defined by (3) indeed sets the lateral scale – with a weak dependence on the inclination angle ϕ. The result obtained for $\phi = 0$ is shown in the inset of Fig. 3 and is accurately described by $\tan\theta \sim e/\ell$, for different f and B, confirming that (3) correctly predicts the lateral scale ℓ.

To explain the nonlinear behaviour of the normal displacement e, we now turn to the freely pending part of the sheet that is not in contact with the gel. The shape is that of a classical elastica, forced by the mass at the end of the tape. Here we parametrise the shape of the tape by $\theta(S)$ relating its local angle to the curvilinear coordinate S (Fig. 2, inset). Introducing the tangential unit vector $\vec{t} = (\cos\theta, \sin\theta)$, the elastica equation can be integrated to

$$\frac{1}{2}B\theta'(S)^2 + \lambda\vec{g}\cdot\left[\vec{t}(S) - \vec{t}(R)\right] = 0, \tag{5}$$

where we used that the end of the tape at $S = R$ is free from torque. At the contact line we can estimate the bending term from the characteristic horizontal and vertical scales: $B\theta'^2 \sim Be^2/\ell^4$. The forcing term in (5) can be written as $\lambda g(1-\sin\phi) = f$, which becomes exact when the pending part of the sheet is long. Combined with (3), this gives the nonlinear scaling for the normal displacement e:

$$\frac{Be^2}{\ell^4} \sim \frac{e^2 G}{\ell} \sim f. \tag{6}$$

This relation is successfully tested in Fig. 2, where we find a collapse over 4 decades, for different inclinations ϕ, for two different bending moduli B, for different gel thicknesses and for different adhesion conditions.

4 Reversibility, work of adhesion and contact angle

The reversibility of the peeling process is illustrated by a series of experiments without an additional mass at the end of the tape. When the pending part of the sheet is sufficiently long, peeling can in fact be induced by the weight of the sheet. However, there is a threshold length below which the surface energy due to adhesion is stronger than gravity, so that the sheet spontaneously reattaches to the gel when its end is released. The resulting peeling velocities v are presented in Fig. 4a, where positive v corre-

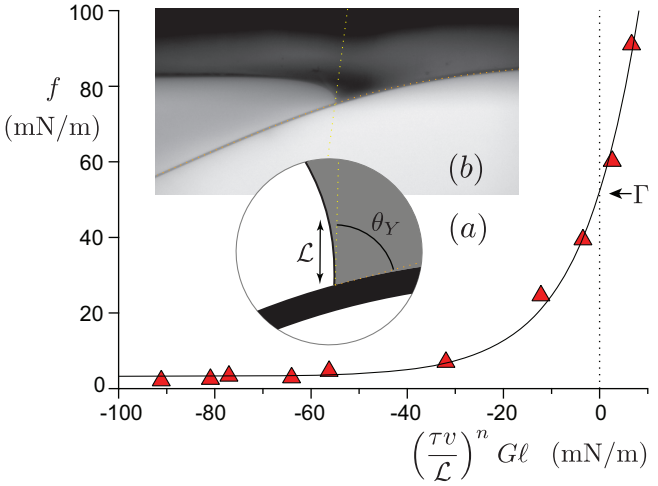

Fig. 4 (a) Relation between the peeling force f and the rescaled velocity v, for the case where no mass is added to the sheet. Data correspond to the metallized film. By convention, we consider that $(-v)^n = -v^n$. The solid line is a guide to the eye. (b) Side view of the gel in the equilibrium condition $f = \Gamma$, showing the Young contact angle $\theta_Y \simeq 65 \pm 5°$.

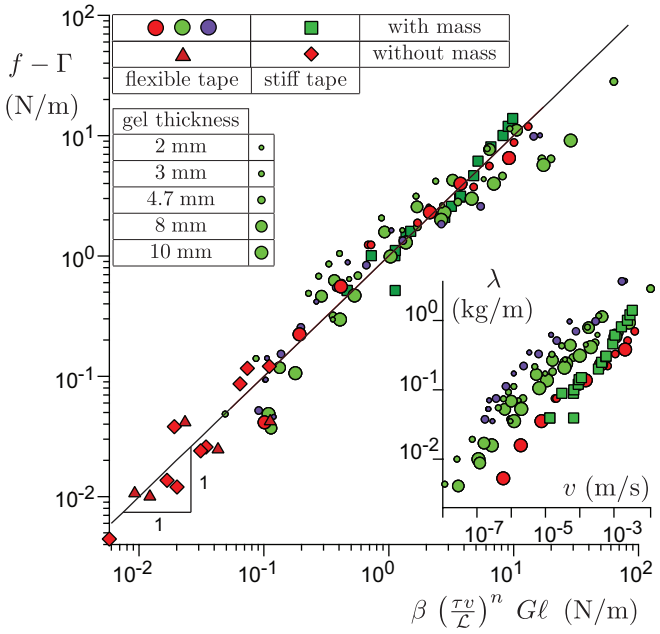

Fig. 5 Relation between the peeling force f and the peeling velocity v, scaled according to (9). The colors correspond to different inclination angles ϕ, from red to blue ($-45°$, $0°$, $45°$) and the symbols to the type of experiment, as shown in the table in inset. The symbol size codes for gel thickness. The inset represents the data without rescaling.

spond to peeling and negative v to reattachment. At the threshold point where $v = 0$, the system is at equilibrium: there is an exact balance between the forcing f and the (conservative) work of adhesion Γ. The values are $\Gamma = 52 \pm 3\,\mathrm{mN.m^{-1}}$ for the metallized sheet and $\Gamma = 19 \pm 3\,\mathrm{mN.m^{-1}}$ for the Mylar sheet. Hence, this experiment allows us to accurately determine the non-dissipative contribution to the adhesion process. Note that reversibility is, here, not intended in the thermodynamic sense (there is a viscoelastic dissipation) but in the structural sense: the adhesive does not present irreversible damages after peeling.

The work of adhesion can be directly related to the shape of the gel on the side that is detached from the sheet. Figure 4b shows that the free surface of the gel is highly curved before contacting the sheet. Just like in a crack *à la* Griffith[36] or in the JKR adhesion problem[37], the normal deflection follows a square root shape $h \sim x^{1/2}$, where x is the horizontal distance measured from the contact line[37]. This square root singularity is the solution of the mixed problem, where a contacting region changes to a stress-free interface. It must not be confused with the logarithmic deformation of a surface submitted to a localized force, which appears here (or in the JKR problem) as the far field solution far away from the contact line[34]. Remarkably, however, the gel is clearly seen to make a well-defined contact angle θ_Y when touching the sheet (Fig. 4b). This strongly resembles the wetting of liquids, for which the work of adhesion can be expressed as $\Gamma = \gamma(1 + \cos\theta_Y)$, where γ is the surface energy of the liquid-vapor interface and θ_Y is Young's contact angle. The gel could indeed obey similar wetting laws[38–40] below the elastocapillary length

$$\mathscr{L} = \frac{\gamma}{G}, \tag{7}$$

where in this case γ is the surface energy of the gel. This length, here approximately $30\,\mu$m, indicates the scale where surface energy dominates over bulk elasticity, and below which we expect "wetting" behavior.

Despite subtleties of capillarity of elastic interfaces[41–43], this wetting interpretation is indeed consistent with our direct measurement of the gel's contact angle. We find $\theta_Y = 65 \pm 5°$ for the metallized sheet, and a higher contact angle $\theta_Y = 125 \pm 5°$ for the less adhesive Mylar sheet. Using the measured Γ and the previously reported value for the surface tension of the gel-vapor interface, $\gamma = 39\,\mathrm{mN.m^{-1}}$[44], the aforementioned relation predicts contact angles of respectively $\theta_Y = 70°$ and $\theta_Y = 120°$, consistent with the measurements.

5 Energy release and dissipation

We now turn to the most important characteristic of the adhesive, namely the relation between the peeling force and the peeling velocity. The unscaled experimental data is shown in the inset of Fig. 5, where we present the mass λ *versus* the velocity v. For each dataset with given tape and inclination ϕ, we find a power law with an exponent 0.53 ± 0.04. Below we demonstrate that this directly reflects the exponent n of the rheology, as given by (1). Another observation is that the peeling velocity is independent of the gel thickness (represented by the size of the symbols), from which we deduce that dissipation is localized in the vicinity of the peeling front.

To interpret the relation between forcing and peeling velocity, we make use of an energy balance. Since inertial effects are negligible, the viscoelastic dissipation in the bulk of the deformed gel must equal the changes in surface energy (due to the work of adhesion) and the forcing by the weight. We thus need to determine the dissipation inside the bulk of the gel layer due to the rheology (1). A closed form expression for the dissipation can be obtained in the limit of small deformations, assuming that the gel

profile (cf. inset Fig. 2) is a traveling wave $h(x-vt)$. The resulting balance reads (see Appendix A):

$$f-\Gamma=\int\frac{dq}{2\pi}\frac{qG''(qv)}{k(q)}|\hat{h}(q)|^2. \quad (8)$$

The integral on the right hand side represents the dissipation, where $\hat{h}(q)$ is the Fourier transform of the gel deformation and $k(q)$ is the spatial Green's function relating deformation to the normal stress. The finite thickness H of the gel layer enters in $k(q)$ for $qH\lesssim 1$. In our case deformation is limited to $\ell\lesssim H$ and we may use the half-space approximation $k(q)\sim(2|q|)^{-1}$; in agreement with the experimentally observed independence of thickness. Naturally, $\omega=qv$ sets the characteristic frequency for the dissipation, as can be seen from the argument of G'' in (8). Furthermore, the independent calibration (1) allows us to write $G''\sim(qv\tau)^nG$.

The final step is to insert the deformation profile $\hat{h}(q)$ in (8). Importantly, when using the crack-shape $h\sim(\ell x)^{1/2}$, for which $\hat{h}\sim\ell^{1/2}/|q|^{3/2}$, the dissipation integral in (8) diverges at large q and gives infinite dissipation at small scales. However, the appearance of a wetting condition at scales below $\sim\mathscr{L}$ provides a cutoff: dissipation becomes integrable when the interface exhibits a finite angle, with details depending on θ_Y. Using $q\sim\mathscr{L}^{-1}$ as the regularisation scale, (8) becomes:

$$f-\Gamma=\beta\left(\frac{\tau v}{\mathscr{L}}\right)^n G\ell. \quad (9)$$

Figure 5 confirms that all data are well-described by (9) with β of order unity. The precise value of β primarily depends on the geometry of the gel at the peeling front: it is found to be ~ 10 times larger for $\theta_Y\simeq 65^\circ$ than for $\theta_Y\simeq 125^\circ$. This illustrates the importance of the contact angle, also for dynamics, since a larger peeling ridge leads to stronger dissipation. β exhibits a subdominant non-monotonic dependence on ϕ that can be traced back to a weak variation of the lateral relaxation scale (see the value of α in Fig. 3).

6 Discussion

While first theories of peeling of pressure sensitive adhesives have described purely static equilibrium situations[12,45], it was soon realised that the peel force was velocity dependent and associated to the rheology of the adhesive[46–49]. The problem of growing cracks in bulk viscoelastic media is closely related, and Schapery[26] predicted a power law dependence of the growth rate of the crack on the applied gross strain, where the exponent is given by the exponent of the creep compliance function. Also closely related is the geometry of a rigid cylinder rolling on a viscoaleastic material, for which a strain energy release rate $\sim v^{0.55}$ has been found[50,51]. Maugis and Barquins[52] showed that peeling of urethane strips off a glass surface yields a power law relation between peeling speed and applied force as well. They attributed this behavior to the rheology of the adhesive since the empiric dissipation relation obeyed the same time-temperature superposition behavior as the loss modulus. They also noticed that, if viscoelastic losses are localized at the crack tip, dissipation was supposed to be geometry independent.

However, to the best of our knowledge, a quantitative theory capable of predicting the peel force for a highly localized dissipation was still missing in literature. Historically, this is most likely due to the fact that typical properties of engineered adhesive tapes lead to characteristic length scales which do not admit such strong localisation: Such tapes typically comprise a thin layer of a soft and highly adherent material, so that the stress localisation $\sim\Gamma/G\sim\mathscr{O}(1\text{ mm})$ is spread much wider than the typical layer thickness $\sim\mathscr{O}(10\ \mu\text{m})$[2,28]. Instead, a cohesive zone forms, composed of fibrils and cavitation bubbles, and the strain energy release rate becomes geometry dependent and typically increases with layer thickness[53]. Those cases clearly require a different type of model, taking the nonlinear rheological properties of the adhesive into account[2,7,10].

The growing interest in reversible adhesives that can be peeled without bulk cavitation or plastic deformations, as inspired e.g. by biology[1,54], suggests revisiting the limit of weakly adherent materials and peeling geometries with localised stress and dissipation. However, the crack singularity of adhesion leads in this case not just to a concentration of the stress to the peeling front, but also to a diverging dissipation in the continuum description. This prevents quantitative predictions unless a physical regularisation mechanism is identified. While the power laws that we find in our experiments are similar to those reported previously[51,52], we could disentangle the various contributions to the peel force by peeling an inextensible flexible tape with different surface energies off a thick elastic layer[55]. Most importantly we have identified solid surface tension and the corresponding "wetting type" boundary condition as the leading order regularisation mechanism for dissipation in reversible peeling.

In conclusion, we have shown that reversible adhesives can indeed obey simple scaling laws for deformation and dissipation, whose origin can be traced back to linear viscoelasticity and, importantly, solid capillarity. Analysing the near-crack-tip geometry, we have shown that the regularisation of elastic singularities by the wetting condition allows one to get quantitative estimates of the viscoelastic dissipation. The theoretical framework proposed here bridges the gap between adhesive peeling and moving contact lines of fluids, opening the possibility of fully quantitative theories. It opens the promising perspective of designing adhesives by coherently tuning their visco-elastic properties, their surface functionalisation, and their meso- and macroscopic architecture.

A The dissipation integral

Here we compute the rate energy dissipation P inside the gel during peeling, which is used to derive equation (8) in the main manuscript. We define the displacement field inside the gel u_i and the stress tensor σ_{ij}. With this, we compute the energy dissipation per unit time (per unit width of the gel) from the usual

integral[56]

$$\begin{aligned} P &= \int d^2x\, \sigma_{ij} \frac{\partial \dot{u}_i}{\partial x_j} \\ &= \int d^2x \left[\frac{\partial}{\partial x_j} \left(\sigma_{ij} \dot{u}_i \right) - \dot{u}_j \frac{\partial \sigma_{ij}}{\partial x_j} \right] \\ &= \oint ds\, \sigma_{ij} n_j \dot{u}_i. \end{aligned} \tag{10}$$

These contain standard manipulations, where we used mechanical equilibrium $\partial \sigma_{ij}/\partial x_j = 0$ and brought the area integral to the boundary with normal vector n_j. The boundary integral represents the work done by normal and tangential tractions. Since the bottom of the gel is fixed to a rigid support ($\dot{u}_i = 0$) the only contribution comes from the free surface. In addition, only the normal traction performs work: the inextensibility of the sheet imposes vanishing tangential displacement, while the tangential stress vanishes on the side that is peeled from the sheet. In the limit of small deformation, the normal displacement can be identified with the gel's profile $h(x,t)$, so that (10) reduces to

$$P = \int_{-\infty}^{\infty} dx\, \sigma(x,t) \dot{h}(x,t), \tag{11}$$

where we denote the normal stress $\sigma = \sigma_{ij} n_i n_j$.

Further progress is made when relating the traction to the normal displacement and the viscoelastic rheology $\mu(\omega) = G'(\omega) + iG''(\omega)$. When taking the Fourier transform in both space ($x \to q$) and time ($t \to \omega$), this can be written as[44,56]

$$\sigma(q,\omega) = \frac{\mu(\omega)}{k(q)} h(q,\omega), \tag{12}$$

where $k(q)$ is the spatial Green's function corresponding to the linear response. Here we implicitly made use that for an incompressible, thick layer normal stress is decoupled from the tangential displacement (see e.g. *Contact Mechanics* by K.L. Johnson). We consider travelling wave solutions

$$\sigma(x,t) = \sigma_c(x - vt) \tag{13}$$

$$h(x,t) = h_c(x - vt), \tag{14}$$

so that

$$\sigma(q,\omega) = \frac{\mu(\omega)}{k(q)} h_c(q)\, 2\pi\delta(\omega - qv) \tag{15}$$

$$\sigma_c(q) = \frac{\mu(qv)}{k(q)} h_c(q). \tag{16}$$

Inserting in (11), the dissipation becomes:

$$\begin{aligned} P &= \int dx \left\{ \int \frac{dq}{2\pi} \frac{\mu(qv)}{k(q)} h_c(q) e^{iq(x-vt)} \right\} \\ &\quad \times \left\{ \int \frac{dq'}{2\pi} (iq'v) h_c(q') e^{iq'(x-vt)} \right\} \end{aligned} \tag{17}$$

We can introduce the variable $\tilde{x} = x - vt$ and perform the x integral using

$$\int d\tilde{x}\, e^{i(q+q')\tilde{x}} = 2\pi\delta(q+q'). \tag{18}$$

This gives a dissipation

$$P = \int \frac{dq}{2\pi} \frac{\mu(qv)}{k(q)} h_c(q) \int \frac{dq'}{2\pi} (iq'v) h_c(q')\, 2\pi\delta(q+q') \tag{19}$$

$$= -v \int \frac{dq}{2\pi} \frac{\mu(qv)}{k(q)} h_c(q)(iq) h_c(-q) \tag{20}$$

$$= -v \int \frac{dq}{2\pi} \frac{\mu(qv)}{k(q)} (iq) |h_c(q)|^2. \tag{21}$$

This expression is real, owing to the symmetry properties $k(q) = k(-q)$ and $\mu(-\omega) = \mu(\omega)^*$, which implies $G'(\omega) = G'(-\omega)$ and $G''(\omega) = -G''(-\omega)$. Hence, as expected, only G'' contributes to the dissipation. Finally, we can define the dissipative force $P = f_d v$. This gives the expression used in equation (8)

$$f_d = \int_{-\infty}^{\infty} \frac{dq}{2\pi} \frac{qG''(qv)}{k(q)} |h_c(q)|^2. \tag{22}$$

B Effect of the weight of the sheet

Here we will derive the expression of the peeling force f, for the experiments where no mass is attached at the end of the tape and for arbitrary lengths of bending tape. The driving force is then due to the weight of the tape and its curvature. To derive the expression, we evaluate the change of the free energy during the peeling, due to contact line motion. It results from two contributions: the variation of the free energy associated to the fact that the total pending length R changes and the variation of the free energy associated with the fact that the contact line position moves accordingly. The contact line position corresponds to the curvilinear coordinate $S = 0$ and the end of the tape is located at $S = R$. Denoting by ρ_S the density per unit tape length, we express the bending energy and gravitational energy of the detached part of the sheet as:

$$\begin{aligned} \mathscr{F} &= \int_0^R dS \frac{1}{2} B \theta'(S)^2 - \int_0^R dS \rho_S \vec{g} \cdot \int_0^S \vec{t}(S') dS' \\ &\quad + \frac{1}{2} \rho_S R^2 g \sin\phi + \mathscr{M}(\theta(0) - \theta_0) \end{aligned} \tag{23}$$

In this expression B is the bending modulus and $\vec{t}$ the tangential vector. The gravitational energy consists of two terms, respectively representing the energy with respect to the contact point (the double integral) and the variation of potential energy associated with the contact translation at an angle ϕ with respect to the horizontal direction (term quadratic in R). The constraint associated to $\mathscr{M}$ imposes the angle of the tape at the contact line ($S=0$) to a value θ_0. $\mathscr{M}$ is therefore the bending moment exerted by the attached part of the tape to the part that is detached. The total variation of the free energy with respect to a change of length R

reads:

$$f = -\frac{\partial \mathscr{F}}{\partial R}. \tag{24}$$

Before turning to $\partial \mathscr{F}/\partial R$, we first consider the minimisation of the total energy with respect to the shape $\delta\theta(S)$. This gives the elastica equation of the tape (without added mass), and the two boundary conditions:

$$0 = B\theta''(S) + \rho_S(R-S)\vec{g}\cdot\frac{d\vec{t}}{d\theta} \tag{25}$$

$$0 = B\theta'(0) - \mathscr{M} \tag{26}$$

$$0 = \theta'(R). \tag{27}$$

Using the boundary conditions this integrates into:

$$\frac{1}{2}B\theta'(S)^2 + \rho_S(R-S)\vec{g}\cdot\vec{t}(S) - \rho_S\vec{g}\cdot\int_S^R \vec{t}(S')dS' = 0. \tag{28}$$

After a straightforward calculation, also making use of the elastic equation, one obtains the variation of free energy as:

$$f = -\rho_S R g(\sin\phi + \sin\theta(0)) + \frac{1}{2}B\theta'(0)^2 + B\theta'\frac{d\theta(0)}{dR}. \tag{29}$$

To obtain f from the experiment, all terms on the right are evaluated directly from the images, where we note that the term $d\theta(0)/dR$ was completely negligible.

Acknowledgments. B.A. is supported by Institut Universitaire de France. This work was funded by the ANR grants Smart. JHS acknowledges financial support from ERC (the European Research Council) Consolidator Grant No. 616918. SK acknowledges financial support from the Max Planck – University of Twente Center 'Complex Fluid Dynamics – Fluid Dynamics of Complexity'.

References

1 D. Labonte and W. Federle, *Phil. Trans. Royal Soc. London B*, 2014, **370**, 20140027.
2 C. Creton and M. Ciccotti, *Rep. Prog. Phys.*, 2016, 046601.
3 L. F. Boesel, C. Greiner, E. Arzt and A. del Campo, *Av. Mater.*, 2010, **22**, 2125–2137.
4 A. Jagota and C.-Y. Hui, *Mater. Sci. Eng. R*, 2011, **72**, 253–292.
5 J. Seo, J. Eisenhaure and S. Kim, *Extreme Mech. Lett.*, 2016, **9**, 207–214.
6 K. Autumn, Y. A. Liang, S. T. Hsieh, W. Zesch, W. P. Chan, T. W. Kenny, R. Fearing and R. J. Full, *Nature*, 2000, **405**, 681–685.
7 T. Vilmin, F. Ziebert and E. Raphaël, *Langmuir*, 2010, **26**, 3257–3260.
8 A. Ghatak and M. K. Chaudhury, *Langmuir*, 2003, **19**, 2621–2631.
9 A. Ghatak, M. K. Chaudhury, V. Shenoy and A. Sharma, *Physical Review Letters*, 2000, **85**, 4329.
10 J. Nase, A. Lindner and C. Creton, *Phys. Rev. Lett.*, 2008, **101**, 074503.
11 J. Teisseire, F. Nallet, P. Fabre and C. Gay, *The Journal of Adhesion*, 2007, **83**, 613–677.
12 D. Kaelble, *Transactions of the Society of Rheology*, 1960, **4**, 45–73.
13 de Gennes, P.G., *J. Phys. France*, 1989, **50**, 2551–2562.
14 P. G. de Gennes, *Langmuir*, 1996, **12**, 4497–4500.
15 de Gennes, P-G., *C. R. Acad. Sc. Paris*, 1988, **307**, 1949.
16 R. A. Schapery, *International Journal of Fracture*, 1975, **11**, 141–159.
17 R. A. Schapery, *International Journal of Fracture*, 1975, **11**, 369–388.
18 C. Hui, D. Xu and E. J. Kramer, *Journal of Applied Physics*, 1992, **72**, 3294–3304.
19 G. Haiat, M. P. Huy and E. Barthel, *Journal of the Mechanics and Physics of Solids*, 2003, **51**, 69 – 99.
20 B. N. J. Persson and E. A. Brener, *Phys. Rev. E*, 2005, 036123.
21 E. Barthel and C. Frétigny, *Journal of Physics D: Applied Physics*, 2009, **42**, 195302.
22 F. Saulnier, T. Ondarçuhu, A. Aradian and E. Raphaël, *Macromolecules*, 2004, 1067–1075.
23 M. Barquins, A. Boilot, M. Ciccotti and A. Varotto, *Comptes rendus de l'Académie des sciences. Série IIb – Mécanique, physique, chimie, astronomie*, 1995, **321**, 393–399.
24 A. N. Gent, *Langmuir*, 1996, **12**, 4492–4496.
25 A. Cristiano, A. Marcellan, B. J. Keestra, P. Steeman and C. Creton, *Journal of Polymer Science Part B: Polymer Physics*, 2011, **49**, 355–367.
26 R. A. Schapery, *International Journal of Fracture*, 1975, **11**, 549–562.
27 P. Rahulkumar, A. Jagota, S. Bennison and S. Saigal, *International Journal of Solids and Structures*, 2000, **37**, 1873–1897.
28 R. Villey, C. Creton, P.-P. Cortet, M.-J. Dalbe, T. Jet, B. Saintyves, S. Santucci, L. Vanel, D. J. Yarusso and M. Ciccotti, *Soft Matter*, 2015, **11**, 3480–91.
29 D. H. Kaelble, *Transactions of the Society of Rheology*, 1965, **9**, 135–163.
30 H. Winter and F. Chambon, *J. Rheol.*, 1986, **30**, 367–382.
31 K. Kendall, *Journal of Adhesion*, 1973, 179–202.
32 L. Benyahia, C. Verdier and J.-M. Piau, *The Journal of Adhesion*, 1997, **62**, 45–73.
33 P.-P. Cortet, M. Ciccotti and L. Vanel, *Journal of Statistical Mechanics: Theory and Experiment*, 2007, **2007**, P03005.
34 G. Miquelard-Garnier, A. B. Croll, C. S. Davis and A. J. Crosby, *Soft Matter*, 2010, **6**, 5789–5794.
35 F. Brau, H. Vandeparre, A. Sabbah, C. Poulard, A. Boudaoud and P. Damman, *Nature Physics*, 2011, 56–60.
36 A. A. Griffith, *Phil. Trans. A*, 1920, **221**, 163–198.
37 K. L. Johnson, K. Kendall and A. D. Roberts, *Proc. R. Soc. London A*, 1971, **324**, 301–313.
38 R. W. Style, C. Hyland, R. Boltyanskiy, J. S. Wettlaufer and E. R. Dufresne, *Nature Comm.*, 2013, **4**, 2728.
39 T. Salez, M. Benzaquen and E. Raphael, *Soft Matter*, 2013, **9**, 10699–10704.
40 S. Karpitschka, L. van Wijngaarden and J. Snoeijer, *Soft Matter*, 2016, **12**, 4463–4471.
41 B. Andreotti and J. H. Snoeijer, *EPL*, 2016, **113**, 66001.
42 B. Andreotti, O. Bäumchen, F. Boulogne, K. E. Daniels, E. R. Dufresne, H. Perrin, T. Salez, J. H. Snoeijer and R. W. Style, *Soft Matter*, 2016, **12**, 2993–2996.
43 R. W. Style, A. Jagota, C.-Y. Hui and E. R. Dufresne, *Annual Review of Condensed Matter Physics*, 2017, **8**, 99–118.
44 S. Karpitschka, S. Das, M. van Gorcum, H. Perrin, B. Andreotti and J. H. Snoeijer, *Nature Commun.*, 2015, **6**, 7891.
45 D. Kaelble, *Transactions of the Society of Rheology*, 1959, **3**, 161–180.
46 D. Kaelble, *J. Coll. Sci.*, 1964, **19**, 413–424.
47 A. N. Gent, *Proc. R. Soc. London A*, 1969, **310**, 433–448.
48 K. Kendall, *Journal of Physics D: Applied Physics*, 1971, **4**, 1186.
49 K. Kendall, *Journal of Physics D: Applied Physics*, 1975, **8**, 1449.
50 M. Barquins, *J. Adhesion*, 1988, **26**, 1–12.
51 F. Robbe-Valloire and M. Barquins, *Int. J. Adhesion Adhesives*, 1998, **18**, 29–34.
52 D. Maugis and M. Barquins, *J. Phys. D: Appl. Phys.*, 1978, **11**, 1989–2023.
53 D. Kaelble, *The Journal of Adhesion*, 1992, **37**, 205–214.
54 A. Ghatak, L. Mahadevan, J. Y. Chung, M. K. Chaudhury and V. Shenoy, Proceedings of the Royal Society of London A: Mathematical, Physical and Engineering Sciences, 2004, pp. 2725–2735.
55 A. Ghatak, L. Mahadevan and M. K. Chaudhury, *Langmuir*, 2005, **21**, 1277–

1281.
56 D. Long, A. Ajdari and L. Leibler, *Langmuir*, 1996, **12**, 1675–1680.